Journal of Fluids and Structures 18 (2003) 165–178

JOURNAL OF FLUIDS AND STRUCTURES

www.elsevier.nl/locate/jnlabr/yjfls

The dynamic response of Coriolis mass flow meters

R. Cheesewright*, C. Clark, A. Belhadj, Y.Y. Hou

Department of Systems Engineering, Brunel University, Uxbridge, Middlesex UB8 3PH, UK

Received 17 February 2003; accepted 30 June 2003

Abstract

The speed of response of commercial Coriolis meters to a step change in mass flow rate corresponds to a time constant which may range from 0.1 s to several seconds. This response is a result both of the dynamic response of the physical components of the meter and of the electronics and the computational algorithms used to convert that dynamic response into an estimate of the mass flow rate. A comprehensive investigation of the dynamic response is presented with a view to establishing the ultimate limits of the overall meter response. Attention is initially concentrated on a simple straight tube meter and analytical solutions are presented for the response to a step change in flow rate both for an undamped meter and for a meter with internal damping. These results are compared with results from a finite element model of the same meter and then the finite element modelling is extended to geometries typical of commercial meters. Finally, representative results are presented from an experimental study of the response of commercial meters to step changes in flow rate. A study of the essential components of the algorithm used in a meter leads to the conclusion that the time constant cannot be less than the period of one cycle of the meter drive. The analytical, finite element and experimental results all combine to show that the meters all respond in the period of one drive cycle but that the flow step induces fluctuations in the meter output which decay under the influence of the flow tube damping. It is the additional damping introduced in the signal processing to overcome these fluctuations which is responsible for the large observed time constants. Possible alternative approaches are discussed.

1. Introduction

In many applications, flow meters are used to determine mean flow rate only, with a time-constant set by the user. There is now however, an increasing need for flow rate measurements in flows which are required to change rapidly with time. This includes short duration batch-flows; for example, delivery of liquid pharmaceuticals into ampoules or perfume into bottles, with batching times less than 1 s. For these measurements, there is a growing need for mass flow meters with a high performance dynamic response. A meter with this capability would also open-up new areas of application, for example, measurement of fuel flow to gas turbine engines, where control loop response times of 20 ms may be required.

The dynamic response of measuring instruments is commonly expressed in terms of a 'time constant' which indicates the time it takes for the instrument to respond to a small step change in the quantity being measured. There appears to be very little published work dealing with the dynamic response of Coriolis meters. A search yielded two papers referring to the response of Coriolis meters to a time dependent flow. One was in the form of a short paper by Cheesewright and Clark (2000), where experimental data were presented to show that, even at pulsation frequencies as low as 5 Hz, there is a large error in the measured pulsation amplitude. The results also show that there is a significant delay following the initiation of a time dependence in the flow before the output signal from the meter shows any

*Corresponding author.
E-mail address: robert.cheesewright@brunel.ac.uk (R. Cheesewright).

0889-9746/$ - see front matter
doi:10.1016/j.jfluidstructs.2003.06.001

change. The other paper, by Wiklund and Peluso (2002) reports the results of frequency response tests on a range of different flow meters including a Coriolis meter. The results are expressed in the form of transfer functions and the Coriolis meter is described as being characterized by 'a critically damped second order lag with a fixed natural frequency and damping ratio, together with a first order lag and a dead time both of which were found to vary with the user selectable damping'. Dead times in the range 30–400 ms are reported with a natural frequency of 2.39 rad/s and a damping ratio of 1.0. These values suggest that an attempt to represent the meter response in terms of a single time constant would lead to a value of the order of 1 s.

The effects of sinusoidal flow pulsations (at frequencies of the order of the meter drive frequency) in degrading the accuracy with which a simple, straight tube, Coriolis meter can measure a mean flow rate have been investigated analytically by Cheesewright and Clark (1998). The results of that investigation were confirmed by Finite Element analyses, both for the simple straight tube meter and for a range of commercially available meters having different geometries, Belhadj et al. (2000). These results were in close accord with the results of experiments on the same meters, Cheesewright et al. (1999). In all these works it was demonstrated that the degradation of meter accuracy occurred because of the generation of additional components in the sensor signals, caused by the flow pulsations. It was further demonstrated that the degree of error depends on the details of the methods used to determine the phase difference between the sensor signals and suggestions were made regarding methods by which the error in the indicated mean flow rate could be reduced. No consideration was, however, given to the question of the extent to which useful information about the time dependence of the flow rate could be recovered from the additional components in the sensor signals.

There are many factors which could influence the overall dynamic response of a Coriolis meter, ranging from the mechanics of the motion of the meter tube to the electronics (signal processing) used to determine the phase difference between the sensor signals and possibly even to the electronics of the feedback system used to maintain the meter drive. The work of Wiklund and Peluso (2002), referred to above, suggests that the signal processing may be the most important factor, with the user selectable damping having a major influence. Some degree of time delay in the meter output reflecting changes in the flow is inevitable because the shortest period over which an estimate of the phase difference can be made is one complete cycle of the meter drive. Thus, if an estimate is associated with the mid point of the period over which it is taken then there must be a delay of at least half the period of a drive cycle. The make and model of Coriolis meter tested by Wiklund and Peluso (2002) is not reported but it is likely to have had a drive frequency of at least 100 Hz which would suggest a minimum delay of the order of 5 ms, which is significantly smaller than the delays which they report.

It is suspected that, for virtually all currently available meters, it is the signal processing which has a controlling influence on the overall response, but the details of the electronics are commercially confidential (to the meter manufacturers). However, in any consideration of what is potentially possible in respect of the dynamic response, it will be the motion of the meter tube relative to the period of one half of a drive cycle which will provide the ultimate limitation. Thus, in the present work, attention will be concentrated on that factor.

2. Formulation and solution of the analytical model

The analytical treatment will use the model presented by Cheesewright and Clark (1998), namely a simple straight tube meter, rigidly fixed at the two ends and driven at its lowest natural frequency.

2.1. Without internal damping

The transverse vibratory motion of the pipe and the fluid is represented by writing the displacement, u, as a function of the distance, x, along the pipe from one end, and of the time, t. Writing force = mass × acceleration for the fluid and recognizing that since $u = u(x, t)$, $\mathrm{d}u/\mathrm{d}t = (\partial u/\partial t) + (\partial u/\partial x)(\mathrm{d}x/\mathrm{d}t) = (\partial u/\partial t) + V(t)(\partial u/\partial x)$, the motion of the fluid is described by

$$m_f \frac{\partial^2 u}{\partial t^2} + 2m_f V \frac{\partial^2 u}{\partial x \partial t} + m_f \frac{\mathrm{d}V}{\mathrm{d}t}\frac{\partial u}{\partial x} + m_f V^2 \frac{\partial^2 u}{\partial x^2} = \lambda, \tag{1}$$

where m_f is the mass of fluid per length of pipe, $V(= V(t))$ is the longitudinal velocity of the fluid and λ is the force per length exerted on the fluid by the constraining pipe. Similarly, the motion of the pipe is described by

$$m_p \frac{\partial^2 u}{\partial t^2} + EI \frac{\partial^4 u}{\partial x^4} = -\lambda, \tag{2}$$

where m_p is the mass per length of the pipe and E and I are respectively the Young's Modulus and the second moment of area of the pipe cross-section.

Eliminating λ between Eqs. (1) and (2) gives the equation of motion of the combined system

$$(m_p + m_f)\frac{\partial^2 u}{\partial t^2} + EI\frac{\partial^4 u}{\partial x^4} + m_f\left[2V\frac{\partial^2 u}{\partial x \partial t} + \frac{dV}{dt}\frac{\partial u}{\partial x} + V^2\frac{\partial^2 u}{\partial x^2}\right] = 0. \tag{3}$$

For a meter of length x the boundary conditions with respect to x are

$$u(0,t) = u(L,t) = 0 \text{ and } \partial u(0,t)/\partial x = \partial u(L,t)/\partial x = 0.$$

Eq. (3) assumes the neglect of axial tensions etc., but it should be noted that Paidoussis and Issid (1974) have suggested that this is not a consistent treatment. They suggest that when such terms are included, the term

$$m_f\frac{dV}{dt}\frac{\partial u}{\partial x}$$

in Eq. (3) should be replaced by

$$m_f\frac{dV}{dt}(L-x)\frac{\partial^2 u}{\partial x^2}.$$

The first objective of the present work is the estimation of the (small) step response of the meter and it is not clear at this stage of the work, whether the disputed term is significant in the estimation of that response.

Regardless of which form of the disputed term is adopted, Eq. (3) is similar to that solved by Raszillier and Durst (1991), in the sense that the first two terms in Eq. (3) will have a dominant influence on the solution. Thus it is reasonable to assume a solution of the form

$$u(x,t) = \sum_{n=1}^{\infty} W_n(x)q_n(t), \tag{4}$$

where the $W_n(x)$ are the mode shapes, obtained from the solution to the equation formed by setting the first two terms in Eq. (3) equal to zero, and the $q_n(t)$ are usually referred to as generalized coordinates. Furthermore, the work of Raszillier and Durst suggests that it should not be necessary to continue the summation beyond the first two or three terms.

For the present boundary conditions, the mode shapes are given by

$$W_n(x) = \sinh(\beta_n x) - \sin(\beta_n x) + \alpha_n[\cosh(\beta_n x) - \cos(\beta_n x)],$$

where $\alpha_n = [\sinh(\beta_n L) - \sin(\beta_n L)]/[\cos(\beta_n L) - \cosh(\beta_n L)]$ and the $\beta_n L$ are the solutions to $\cos(\beta_n L)\cosh(\beta_n L) = 1$. For the case of $V = 0$ the generalized coordinates are given by $q_n(t) = \sin(\omega_n t)$, where ω_n is the natural frequency of the nth mode of vibration and is defined by $\omega_n = (\beta_n L)^2[EI/L^4(m_p + m_f)]^{1/2}$. When the assumed form of solution is substituted into Eq. (3), after some re-arrangement, the equation can be written as

$$0 = \sum_{n=1}^{\infty}\omega_n^2 W_n(x)q_n(t) + \sum_{n=1}^{\infty} W_n(x)\frac{d^2 q_n(t)}{dt^2} + \frac{m_f}{(m_p + m_f)} \times \left(2V\sum_{n=1}^{\infty}\frac{dW_n(x)}{dx}\frac{dq_n(t)}{dt} + \frac{dV}{dt}\sum_{n=1}^{\infty}\frac{dW_n(x)}{dx}q_n(t) + V^2\sum_{n=1}^{\infty}\frac{d^2 W_n(x)}{dx^2}q_n(t)\right), \tag{5}$$

or, if the Paidoussis and Issid (1974) form of the equation had been used,

$$0 = \sum_{n=1}^{\infty}\omega_n^2 W_n(x)q_n(t) + \sum_{n=1}^{\infty} W_n(x)\frac{d^2 q_n(t)}{dt^2} + \frac{m_f}{(m_p + m_f)} \times \left(2V\sum_{n=1}^{\infty}\frac{dW_n(x)}{dx}\frac{dq_n(t)}{dt} + \frac{dV}{dt}(L-x)\sum_{n=1}^{\infty}\frac{dW_n^2(x)}{dx^2}q_n(t) + V^2\sum_{n=1}^{\infty}\frac{d^2 W_n(x)}{dx^2}q_n(t)\right). \tag{5a}$$

Multiplying Eq. (5) (or Eq. (5a)) through by the general mode shape $W_m(x)$, integrating with respect to x from $x = 0$ to $x = L$ and imposing the condition of orthogonality of normal modes gives, for mode m

$$0 = \frac{\partial^2 q_m(t)}{\partial t^2} + \omega_m^2 q_m(t) + \frac{m_f}{(m_p + m_f)} \frac{1}{\int_0^L W_m^2(x)\,\mathrm{d}x} \left[2V \sum_{n=1}^{\infty} \left\{ \frac{\mathrm{d}q_n(t)}{\mathrm{d}t} \int_0^L W_m(x) \frac{\mathrm{d}W_n(x)}{\mathrm{d}x}\,\mathrm{d}x \right\} + \frac{\mathrm{d}V}{\mathrm{d}t} \sum_{n=1}^{\infty} \left\{ q_n(t) \int_0^L W_m(x) \frac{\mathrm{d}W_n(x)}{\mathrm{d}x}\,\mathrm{d}x \right\} + V^2 \sum_{n=1}^{\infty} \left\{ q_n(t) \int_0^L W_m(x) \frac{\mathrm{d}^2 W_n(x)}{\mathrm{d}x^2}\,\mathrm{d}x \right\} \right], \tag{6}$$

or, if the Paidoussis and Issid (1974) form of the equation had been used,

$$0 = \frac{\partial^2 q_m(t)}{\partial t^2} + \omega_m^2 q_m(t) + \frac{m_f}{(m_p + m_f)} \frac{1}{\int_0^L W_m^2(x)\,\mathrm{d}x} \left[2V \sum_{n=1}^{\infty} \left\{ \frac{\mathrm{d}q_n(t)}{\mathrm{d}t} \int_0^L W_m(x) \frac{\mathrm{d}W_n(x)}{\mathrm{d}x}\,\mathrm{d}x \right\} + \frac{\mathrm{d}V}{\mathrm{d}t} \sum_{n=1}^{\infty} \left\{ q_n(t) \int_0^L W_m(x)(L-x) \frac{\mathrm{d}^2 W_n(x)}{\mathrm{d}x^2}\,\mathrm{d}x \right\} + V^2 \sum_{n=1}^{\infty} \left\{ q_n(t) \int_0^L W_m(x) \frac{\mathrm{d}^2 W_n(x)}{\mathrm{d}x^2}\,\mathrm{d}x \right\} \right]. \tag{6a}$$

Eq. (6) (or Eq. (6a)) describes an infinite set of coupled equations for the generalized coordinates. The following coefficients can be defined in terms of the mode shape integrals, which appear in these equations:

$$\theta_m = \frac{1}{L} \int_0^L W_m^2(x)\,\mathrm{d}x, \psi_{m,n} = \int_0^L W_m(x) \frac{\mathrm{d}W_n(x)}{\mathrm{d}x}\,\mathrm{d}x,$$

$$\chi_{m,n} = L \int_0^L W_m(x) \frac{\mathrm{d}^2 W_n(x)}{\mathrm{d}x^2}\,\mathrm{d}x, \quad \sigma_{m,n} = \int_0^L x W_m(x) \frac{\mathrm{d}W_n(x)}{\mathrm{d}x}\,\mathrm{d}x.$$

These coefficients have been evaluated up to $m = n = 6$. Values of θ_m, $\psi_{m,n}$ and $\chi_{m,n}$ are given in Table 1 of Cheesewright and Clark (1998) and it will be seen below that only the values of $\sigma_{2,1}$ and $\sigma_{2,2}$ (0.0006 and −22.9893) are needed in the present work. A full table of values of $\sigma_{m,n}$ is available from the authors. The work of Raszillier and Durst (1991) and the extensions to that work by Raszillier et al. (1993), suggest that a good approximation can be obtained by considering only the first two modes of the series. Introducing this approximation, Eq. (6) yields the following pair of equations for the generalized coordinates q_1 and q_2 (in which the explicit designation of the dependent variable has been dropped and terms, which are identically zero, have been omitted:

$$\frac{\mathrm{d}^2 q_1}{\mathrm{d}t^2} + \omega_1^2 q_1 + \frac{m_f}{L\theta_1(m_p + m_f)} \left[2\psi_{1,2} V \frac{\mathrm{d}q_2}{\mathrm{d}t} + \psi_{1,2} \frac{\mathrm{d}V}{\mathrm{d}t} q_2 + \frac{V^2}{L} \chi_{1,1} q_1 \right] = 0, \tag{7}$$

$$\frac{\mathrm{d}^2 q_2}{\mathrm{d}t^2} + \omega_2^2 q_2 + \frac{m_f}{L\theta_2(m_p + m_f)} \left[2\psi_{2,1} V \frac{\mathrm{d}q_1}{\mathrm{d}t} + \psi_{2,1} \frac{\mathrm{d}V}{\mathrm{d}t} q_1 + \frac{V^2}{L} \chi_{2,2} q_2 \right] = 0, \tag{8}$$

or

$$\frac{\mathrm{d}^2 q_2}{\mathrm{d}t^2} + \omega_2^2 q_2 + \frac{m_f}{L\theta_2(m_p + m_f)} \left[2\psi_{2,1} V \frac{\mathrm{d}q_1}{\mathrm{d}t} - \frac{\mathrm{d}V}{\mathrm{d}t} (\sigma_{2,1} q_1 + (\chi_{2,2} - \sigma_{2,2}) q_2) + \frac{V^2}{L} \chi_{2,2} q_2 \right] = 0. \tag{8a}$$

A study of the results of Raszillier and Durst suggests that for all practical Coriolis meters, q_2 is between 100 and 1000 times smaller than q_1.

Eq. (7) can be written as

$$\frac{\mathrm{d}^2 q_1}{\mathrm{d}t^2} + q_1 \left[\omega_1^2 + \frac{\chi_{1,1} m_f V^2}{L^2 \theta_1 (m_p + m_f)} \right] = -\frac{\psi_{1,2} m_f}{L\theta_1(m_p + m_f)} \left[2V \frac{\mathrm{d}q_2}{\mathrm{d}t} + \frac{\mathrm{d}V}{\mathrm{d}t} q_2 \right]. \tag{9}$$

The solution to Eq. (9) is of the form

$$q_1 = C_{1,0} \sin(\gamma_1 t) + C_{1,1} \cos(\gamma_1 t) + \{\text{particular integral}\}, \tag{10}$$

where

$$\gamma_1 = \sqrt{\omega_1^2 + \frac{\chi_{1,1} m_f V^2}{L^2 \theta_1 (m_p + m_f)}}.$$

The meter is driven at a frequency γ_1, by a feedback system and this fact, together with the fact that $q_2 \ll q_1$ suggests that Eq. (10) can be approximated as

$$q_1 = C_{1,0} \sin(\gamma_1 t), \tag{11}$$

where the origin of the time scale has been chosen so that $C_{1,1} = 0$.

Before Eq. (11) is substituted into Eqs. (8) and (8a) it is appropriate to examine the relative magnitudes of the coefficients of the $\mathrm{d}V/\mathrm{d}t$ terms in the two equations. In Eq. (8) the $\mathrm{d}V/\mathrm{d}t$ term could be significant relative to the V term for rapid changes of flow and we should retain the term. In Eq. (8a) however, both components of the coefficient of the $\mathrm{d}V/\mathrm{d}t$ term are two to three orders of magnitude smaller, even for rapid changes in flow. Thus, if the Paidoussis and Issid form of the governing equation is followed, the $\mathrm{d}V/\mathrm{d}t$ term can be ignored for the present problem.

Substituting from Eq. (11) into Eq. (8), this equation can be written as

$$\frac{\mathrm{d}^2 q_2}{\mathrm{d}t^2} + \gamma_2^2 q_1 = -\frac{C_{1,0} \psi_{2,1} m_f}{L \theta_2 (m_p + m_f)} \left[2V\gamma_1 \cos(\gamma_1 t) + \frac{\mathrm{d}V}{\mathrm{d}t} \sin(\gamma_1 t) \right], \tag{12}$$

where

$$\gamma_2 = \sqrt{\omega_2^2 + \frac{\chi_{2,2} m_f V^2}{L^2 \theta_2 (m_p + m_f)}}.$$

In the examination of the dynamic response of a Coriolis meter we need to explore the solution to Eq. (12) for the case of

$$V = V_0 + H(t - t_0)\delta V, \tag{13}$$

where $H(t - t_0)$ is the Heaviside unit function defined as $H(t - t_0) = 0$ for $t < t_0$ and $H(t - t_0) = 1$ for $t \geqslant t_0$.

The solution to Eq. (12) under these conditions is

$$\begin{aligned} q_2 = {} & C_{2,0} \sin(\gamma_2 t) + C_{2,1} \cos(\gamma_2 t) - \frac{2\psi_{2,1} C_{1,0} \gamma_1 m_f \cos(\gamma_1 t)}{L \theta_2 (m_p + m_f)(\gamma_2^2 - \gamma_1^2)} (V_0 + H(t - t_0)\delta V) \\ & + \frac{C_{1,0} m_f H(t - t_0)}{L \theta_2 (m_p + m_f)(\gamma_2^2 - \gamma_1^2)} \left[\frac{\psi_{2,1}(\gamma_2 + \gamma_1) + 2\psi_{2,1}\gamma_1 \cos(\gamma_2 t - \gamma_2 t_0 - \gamma_1 t_0)}{\gamma_2(\gamma_2 + \gamma_1)} \right. \\ & \left. - \frac{\psi_{2,1}(\gamma_2 - \gamma_1) - 2\psi_{2,1}\gamma_1 \cos(\gamma_2 t - \gamma_2 t_0 + \gamma_1 t_0)}{\gamma_2(\gamma_2 - \gamma_1)} \right]. \end{aligned} \tag{14}$$

In Eq. (14) the constants $C_{2,0}$ and $C_{2,1}$ depend on whether the meter is driven at zero flow and then the flow is switched on (at V_0) or the flow is started and then the meter drive is switched on.

It is clear from Eq. (14) that, in the absence of damping, the solution does not predict any delay mechanism in the response to a step change. It can also be inferred from this solution that the response to a flow impulse (period $\ll 1/\gamma_1$) would be merely an increase in the level of the γ_2 component in the sensor signals.

Commercial Coriolis meters do exhibit internal damping and estimates of the magnitude of that damping, expressed as a percentage of the 'critical' damping, have been obtained both from tests in which the meter drive was suddenly switched off and the decay of the tube motion was recorded, and from finite element computations of model meters. Details of both of these estimates are given in a paper by Cheesewright et al. (2003). It is therefore necessary to revise the present model of a simple straight tube meter to include the effects of damping.

2.2. With the inclusion of the effect of internal damping

Clough and Penzien (1975) describe two different mechanisms by which viscous (i.e. velocity dependent) damping can occur in a beam. These mechanisms are described respectively as, a viscous resistance to transverse displacement of the beam and a viscous resistance to straining of the beam material. However, the second of these is usually very much smaller than the first and there is relatively little information on appropriate values of the coefficient which occurs in the formulation of the mechanism. In addition, finite element simulations using the ANSYS program, normally only model the first damping mechanism. Thus only the first mechanism will be considered and this adds an extra term to

Eq. (2), giving

$$m_p\frac{\partial^2 u}{\partial t^2}+EI\frac{\partial^4 u}{\partial x^4}+c_sI\frac{\partial^5 u}{\partial x^4\partial t}=-\lambda, \tag{15}$$

where c_s is the coefficient of resistance to strain velocity.

Eliminating λ between Eqs. (1) and (15) gives the equation of motion of the combined system including the effects of material damping, but neglecting the influence of axial forces and the suggestions of Paidoussis and Issid (1974):

$$(m_p+m_f)\frac{\partial^2 u}{\partial t^2}+EI\frac{\partial^4 u}{\partial x^4}+c_sI\frac{\partial^5 u}{\partial x^4\partial t}+m_f\left[2V\frac{\partial^2 u}{\partial x\partial t}+\frac{\mathrm{d}V}{\mathrm{d}t}\frac{\partial u}{\partial x}+V^2\frac{\partial^2 u}{\partial x^2}\right]=0. \tag{16}$$

When this equation is subjected to the solution procedure used for the undamped case, the equivalent of Eq. (6) is

$$\begin{aligned}0=&\frac{\partial^2 q_m(t)}{\partial t^2}+\omega_m^2 q_m(t)+\omega_m^2\frac{c_s}{E}\frac{\mathrm{d}q_m}{\mathrm{d}t}\\&+\frac{m_f}{(m_p+m_f)}\frac{1}{\int_0^L W_m^2(x)\,\mathrm{d}x}\left[2V\sum_{n=1}^{\infty}\left\{\frac{\mathrm{d}q_n(t)}{\mathrm{d}t}\int_0^L W_m(x)\frac{\mathrm{d}W_n(x)}{\mathrm{d}x}\mathrm{d}x\right\}\right.\\&\left.+\frac{\mathrm{d}V}{\mathrm{d}t}\sum_{n=1}^{\infty}\left\{q_n(t)\int_0^L W_m(x)\frac{\mathrm{d}W_n(x)}{\mathrm{d}x}\mathrm{d}x\right\}+V^2\sum_{n=1}^{\infty}\left\{q_n(t)\int_0^L W_m(x)\frac{\mathrm{d}^2W_n(x)}{\mathrm{d}x^2}\mathrm{d}x\right\}\right].\end{aligned} \tag{17}$$

Assuming that the expansion can be truncated after the first two modes and introducing the previously defined symbolic representations of the relevant mode shape integrals, the generalized coordinates, q_1 and q_2, can be represented by the following pair of equations:

$$\frac{\mathrm{d}^2 q_1}{\mathrm{d}t^2}+\omega_1^2 q_1+\omega_1^2\frac{c_s}{E}\frac{\mathrm{d}q_1}{\mathrm{d}t}+\frac{m_f}{L\theta_1(m_p+m_f)}\left[2\psi_{1,2}V\frac{\mathrm{d}q_2}{\mathrm{d}t}+\psi_{1,2}\frac{\mathrm{d}V}{\mathrm{d}t}q_2+\frac{V^2}{L}\chi_{1,1}q_1\right]=0, \tag{18}$$

$$\frac{\mathrm{d}^2 q_2}{\mathrm{d}t^2}+\omega_2^2 q_2+\omega_2^2\frac{c_s}{E}\frac{\mathrm{d}q_2}{\mathrm{d}t}+\frac{m_f}{L\theta_2(m_p+m_f)}\left[2\psi_{2,1}V\frac{\mathrm{d}q_1}{\mathrm{d}t}+\psi_{2,1}\frac{\mathrm{d}V}{\mathrm{d}t}q_1+\frac{V^2}{L}\chi_{2,2}q_2\right]=0. \tag{19}$$

In order to maintain consistency with the solution for the undamped case, Eq. (18) can be re-written as

$$\frac{\mathrm{d}^2 q_1}{\mathrm{d}t^2}+\gamma_1^2 q_1+\gamma_1^2\frac{c_s}{E}\frac{\mathrm{d}q_1}{\mathrm{d}t}+\frac{m_f}{L\theta_1(m_p+m_f)}\left[2\psi_{1,2}V\frac{\mathrm{d}q_2}{\mathrm{d}t}+\psi_{1,2}\frac{\mathrm{d}V}{\mathrm{d}t}q_2\right]=0, \tag{20}$$

where, as before

$$\gamma_1=\sqrt{\omega_1^2+\frac{\chi_{1,1}m_fV^2}{L^2\theta_1(m_p+m_f)}}$$

and the ω_1^2 in the third term has been replaced by γ_1^2 because the difference between ω_1 and γ_1 is small and the third term is small compared to the other terms in the equation.

The fact that the meter is driven at a frequency γ_1, via a feedback system, together with the fact that $q_2 \ll q_1$ suggests that the solution to Eq. (20) can be approximated as

$$q_1=C_{1,0}\sin(\gamma_1 t), \tag{21}$$

where the origin of the time scale has been chosen so that $C_{1,1}=0$.

Substituting from Eq. (21) into Eq. (19) gives

$$\frac{\mathrm{d}^2 q_2}{\mathrm{d}t^2}+\gamma_2^2 q_2+\omega_2^2\frac{c_s}{E}\frac{\mathrm{d}q_2}{\mathrm{d}t}=-\frac{C_{1,0}\psi_{2,1}m_f}{L\theta_2(m_p+m_f)}\left[2V\gamma_1\cos(\gamma_1 t)+\frac{\mathrm{d}V}{\mathrm{d}t}\sin(\gamma_1 t)\right], \tag{22}$$

where, as before, γ_2 is defined by

$$\gamma_2 = \sqrt{\omega_2^2 + \frac{\chi_{2,2} m_f V^2}{L^2 \theta_2 (m_p + m_f)}}.$$

Substitution of typical values into Eq. (22) suggests that the difference between ω_2 and γ_2 is less than 0.1% of their value so that we may replace the ω_2^2 in the third term by γ_2^2.

In order to simplify the discussion of the solution of Eq. (22) under the influence of rapid flow transients it is convenient to define

$$K_2 = \frac{C_{1,0} \psi_{2,1} m_f}{L \theta_2 (m_p + m_f)},$$

so that Eq. (22) can be written as

$$\frac{d^2 q_2}{dt^2} + \omega_2^2 \frac{c_s}{E} \frac{dq_2}{dt} + \gamma_2^2 q_2 = -K_2 \left[2V\gamma_1 \cos(\gamma_1 t) + \frac{dV}{dt} \sin(\gamma_1 t) \right]. \tag{23}$$

The available experimental data on the magnitude of the material damping are largely expressed in terms of the ratio, α_1, of the actual damping to the critical damping for the first mode motion (e.g. Cheesewright et al., 2003; Hulbert et al., 1995; Cunningham, 1994). From Eq. (20) it can be seen that the critical damping is obtained for the first mode motion when $c_s = 2E/\gamma_1$ so that in general $c_s = 2\alpha_1 E/\gamma_1$. Substituting into Eq. (23) gives

$$\frac{d^2 q_2}{dt^2} + 2\alpha_2 \gamma_2 \frac{dq_2}{dt} + \gamma_2^2 q_2 = -K_2 \left[2V\gamma_1 \cos(\gamma_1 t) + \frac{dV}{dt} \sin(\gamma_1 t) \right], \tag{24}$$

where α_2 is the damping ratio for the second mode motion, defined by $\alpha_2 = \alpha_1 \gamma_2 / \gamma_1$.

Before examining the effect of a step change in the flow rate it is of interest to examine the influence of material damping on the normal behaviour of the meter. While it is possible to obtain an exact solution to Eq. (24), it is more convenient to make an approximation on the basis of typical values of α_2, γ_2 and γ_1. The sources noted above suggest that α_1 is typically between 4.5×10^{-3} and 3×10^{-4}. For the range of commercial meters which the authors have tested, γ_2 is between 10^3 and 1.4×10^4 and γ_2 for the simple straight tube meter is also within this range (typical values of γ_1 range between 5×10^2 and 5×10^3). The solution to Eq. (24) is made easier if we write it as

$$\frac{d^2 q_2}{dt^2} + 2\alpha_2 \gamma_2 \frac{dq_2}{dt} + \gamma_2^2 (1 + \alpha_2^2) q_2 = -K_2 \left[2V\gamma_1 \cos(\gamma_1 t) + \frac{dV}{dt} \sin(\gamma_1 t) \right], \tag{25}$$

and the error introduced by the additional term is completely negligible.

For a steady flow velocity, V, the solution to Eq. (25) is given by

$$\begin{aligned} q_2 = {} & e^{-\alpha_2 \gamma_2 t} [C_{2,0} \sin(\gamma_2 t) + C_{2,1} \cos(\gamma_2 t)] \\ & - 2V\gamma_1 K_2 \frac{2\alpha_2 \gamma_2 \gamma_1 \sin(\gamma_1 t) + (\gamma_2^2 + \alpha_2^2 \gamma_2^2 - \gamma_1^2) \cos(\gamma_1 t)}{(1 + \alpha_2^2)^2 \gamma_2^4 + 2(\alpha_2^2 - 1) \gamma_2^2 \gamma_1^2 + \gamma_1^4}. \end{aligned} \tag{26}$$

On the basis of the typical values of α_2, γ_2 and γ_1 noted above, this can be further approximated to

$$q_2 = e^{-\alpha_2 \gamma_2 t} [C_{2,0} \sin(\gamma_2 t) + C_{2,1} \cos(\gamma_2 t)] - \frac{2V\gamma_1 K_2}{(\gamma_2^2 - \gamma_1^2)} \cos(\gamma_1 t), \tag{27}$$

and we see that to a high degree of approximation, the only effect of the damping on the steady flow performance of a meter is to cause the terms in $\sin(\gamma_2 t)$ and $\cos(\gamma_2 t)$, which arise from the initial conditions, to decay (the damping will, of course, increase the power input required to drive the meter). This behaviour is in agreement with the results of finite element simulations of steady flow through meters with damping.

Returning to the problem of the step response of a meter with damping, we can retain the approximation made to the last term on the l.h.s. of Eq. (24) and we are thus interested in the solution to Eq. (25) for the case where $V(t) = V_0 + H(t - t_0)\delta V$.

The solution now is

$$q_2 = e^{-\alpha_2\gamma_2 t}[C_{2,0}\sin(\gamma_2 t) + C_{2,1}\cos(\gamma_2 t)] - 2[V_0 + H(t-t_0)\delta V]\gamma_1 K_2 \times \frac{2\alpha_2\gamma_2\gamma_1\sin(\gamma_1 t) + (\gamma_2^2 + \alpha_2^2\gamma_2^2 - \gamma_1^2)\cos(\gamma_1 t)}{(1+\alpha_2^2)^2\gamma_2^4 + 2(\alpha_2^2-1)\gamma_2^2\gamma_1^2 + \gamma_1^4} - \frac{2H(t-t_0)\delta V\gamma_1 K_2 e^{-\alpha_2\gamma_2 t}}{(1+\alpha_2^2)^2\gamma_2^4 + 2(\alpha_2^2-1)\gamma_2^2\gamma_1^2 + \gamma_1^4} \times [(\gamma_2^2(1+\alpha_2^2) + 2\gamma_2\gamma_1 + \gamma_1^2)(\alpha_2\gamma_2\sin(\gamma_2(t-t_0) + \gamma_1 t_0) + (\gamma_2 - \gamma_1)\cos(\gamma_2(t-t_0) + \gamma_1 t_0)) + (\gamma_2^2(1+\alpha_2^2) - 2\gamma_2\gamma_1 + \gamma_1^2)(\alpha_2\gamma_2\sin(\gamma_2(t-t_0) - \gamma_1 t_0) + (\gamma_2 - \gamma_1)\cos(\gamma_2(t-t_0) - \gamma_1 t_0))]. \quad (28)$$

Eq. (28) looks very complicated but when it is examined carefully it can be seen that the terms on the first line represent decaying oscillations at frequency γ_2 which arise from the start-up conditions; the term on the second line is identical to that obtained in the damped steady state solution (Eq. (26)) except that V is replaced by $V_0 + H(t-t_0)\delta V$, and the remaining terms represent decaying oscillations at frequency γ_2, arising from the step. When Eq. (28) is simplified on the basis of the typical values of α_2, γ_2 and γ_1 the solution becomes

$$q_2 = e^{-\alpha_2\gamma_2 t}[C_{2,0}\sin(\gamma_2 t) + C_{2,1}\cos(\gamma_2 t)] - \frac{2[V_0 + H(t-t_0)\delta V]\gamma_1 K_2}{(\gamma_2^2 - \gamma_1^2)}\cos(\gamma_1 t) - \frac{2H(t-t_0)\delta V\gamma_1(\gamma_2 - \gamma_1)K_2 e^{-\alpha_2\gamma_2 t}}{\gamma_2}\left[(\cos(\gamma_2(t-t_0) + \gamma_1 t_0)) + \frac{(\gamma_2 - \gamma_1)}{(\gamma_2 + \gamma_1)}\cos(\gamma_2(t-t_0) - \gamma_1 t_0)\right]. \quad (29)$$

If the Paidoussis and Issid formulation had been followed it would not have changed the essential characteristics of Eqs. (28) and (29).

The solutions show that, within the level of approximation used above, the 'Coriolis' term is not subject to any damping although the terms at the γ_2 frequency are subject to damping. The physical explanation of this result is that the 'Coriolis' term is driven by the first mode motion, which we have assumed to be unaffected by damping (because of the drive). The extent to which the above result will be reproduced in real meters may be affected by the details of the feedback mechanism used to generate the drive signal but these details are commercially confidential and are not available to the authors of this study.

The above analysis has been performed for the simplest possible straight tube meter, driven at its lowest natural frequency. Since a majority of commercially available meters do not have this geometry, it is important to examine the influence of the tube geometry. The finite element models of commercial meters, described by Belhadj et al. (2000) can be used for such an examination.

3. Formulation and solution of the finite element model

Full details of the finite element treatment, the models of a number of different commercially available meters and of the method of solution are given in Belhadj et al. (2000). The general purpose ANSYS code was used and the 3-D mass, stiffness and damping elements were based both on the steady flow work of Stack et al. (1993) and the theoretical equations of motion given by Paidoussis and Issid (1974). The detailed behaviour of the flow within the tube was assumed to have a negligibly small effect on the overall response, so the fluid was treated as a frictionless solid mass travelling along the tube at a velocity which could vary with time. This time dependence was imposed by using the "element birth and death" feature of ANSYS.

The meters which were modelled in the work comprised a straight single tube meter and three twin tube meters which are referred to as the α-tube meter, the Ω-tube meter and the B-tube meter. For all four meters the physical dimensions of the tube and the material properties were supplied by the respective meter manufacturer. The models did not include any additional components which may be attached to specific points on the tubes of the commercial meters. The straight tube meter was only partially based on a commercial meter and was configured to enable a direct comparison between the finite element predictions and the analytical predictions. The accuracy of the finite element modelling was demonstrated by very close agreement between the predicted resonant mode frequencies and those determined experimentally, as reported by Belhadj et al. (2000) and by Cheesewright et al. (2003).

The computations of the step response were based on a "standard" flow rate of 2.62 kg/s for all of the meters. Three flow steps were considered for each meter, zero flow to the standard flow, the standard flow to zero and a small step up from the standard flow. Although all the meters were nominally 25 mm, the actual internal diameters of the tubes varied from one meter to another. The flow velocities corresponding to the "standard" flow were 7.0, 4.41, 7.21 and 5.44 m/s for the straight tube, the α-tube, the Ω-tube and the B-tube meters, respectively. All the transient calculations were started by imposing a pure driven motion (i.e. without any Coriolis distortion). The first stage of the calculations was

performed with a high computational damping (damping ratio of 0.5% which is 10 × the ANSYS default damping) and were run until the effect of the initial transients had decayed to a negligible amplitude (45–85 cycles of the driven motion depending on the particular meter). The output of the first stage calculation was recorded and was used to start the main transient calculation, which was performed for a number of different values of the damping ratio (including the experimentally determined value for each meter, as reported by Cheesewright et al. (2003). The displacement time histories of the sensor mounting points were extracted from the main calculation and these time histories were then processed, using the algorithms that were developed at Brunel for processing experimental data, to give time histories of the phase difference between the two simulated sensor signals. Segments of the displacement time histories were also subjected to spectral analysis.

4. Experimental test facility

The flow test facility is powered by a positive displacement pump, driven at a constant speed, which delivers a flow of 8.7 kg/s (water) at a pressure of 20 bar. The flow to the test section is delivered via a high resistance pipe section and the flow rate is controlled (in the range 0.2–8.7 kg/s) by bleeding off a part of the flow. The steady state pressure varied with flow rate and was in the range 0.2–1.1 bar. The test section comprises a bypass, where the flow is controlled by a valve and/or a burstable diaphragm, and a main section where the meter under test is mounted between a specially modified electro-magnetic flow meter and a variable area orifice. Schematic representation of the arrangement is shown in Fig. 1.

Two methods are provided for generating 'step' changes in flow rate. In the first, a variable area orifice plate is moved at speed across the flow, either increasing or decreasing the effective orifice area and hence the flow rate. This mechanism is located just downstream of the Coriolis meter under test and it allows for relatively large 'step' changes in flow e.g. from 0.2 to 0.8 kg/s over intervals which can be as small as 4 ms.

However, the orifice plate device generates considerable mechanical vibration while producing the step change in flow. The second method uses the sudden opening of a by-pass line to produce smaller reductions in the flow rate through the meter. The sudden opening is produced by the bursting of a thin plastic diaphragm covering the free end of the liquid filled by-pass. The bursting is initiated by applying a sudden discharge of electrical energy through a high resistance coil in contact with the diaphragm. This mechanism produces relatively slow 'steps' (approximately 100 ms) with very low levels of vibration.

Additional instrumentation is provided to enable full characterization of the dynamic features of the flow step. A commercial electromagnetic flow meter provides a clear indication of the time history of the step. The meter is excited

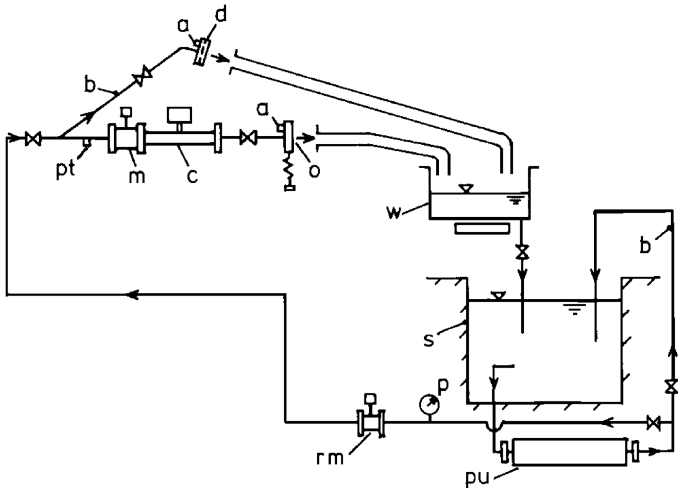

a accelerometer | b by-pass | c Coriolis test meter
d burstable diaphragm | m electromagnetic flowmeter | o variable area orifice
p pressure gauge | pt pressure transducer | pu pump
rm reference flowmeter | s sump | w weigh-tank

Fig. 1. Flow test facility.

by a continuous DC magnetic field which gives a very good dynamic response but at the expense of a poor steady state response due to polarization effects at the sensor electrodes. A pressure transducer is located just upstream of the two flow meters and accelerometers are mounted adjacent to the flow step mechanisms. The accelerometer signals are arranged to have a small dc component and the first zero crossing is used to trigger the collection of data and for the synchronization between the two computers used for data logging.

The first computer logs four channels of data, namely: pressure, accelerometer signal, flow rate indicated by the electromagnetic meter and the flow rate indicated by the Coriolis meter under test. This latter signal is taken either from the current output or the frequency output depending on the advice of the meter manufacturer as to which they expect to give the cleanest, fastest response. The sampling rate on this first computer is typically 51.2 kHz for a 5 s record. The second computer logs the two sensor signals from the test meter at a sampling rate of 500 kHz for a 1.95 s record. The logging programs and the subsequent off-line processing are performed using the LABVIEW system, with the two sensor signals yielding an independent time history of the phase difference.

In general the two sensor signals contain components at a number of different frequencies although the dominant component is that at the meter drive frequency. However, it has been clearly demonstrated by Cheesewright et al. (1999) and by Clark and Cheesewright (2003) that it is only the phase difference between the drive frequency components of the signals which is proportional to the mass flow rate. The computation of the phase difference between the signals can only be made over a period of time which corresponds to an integer number of cycles of the drive frequency, because a computation over any other period would require an a priori knowledge of the shape of the signal waveform at that frequency. Such a knowledge cannot be available and indeed it is flow rate dependent. Thus the shortest period over which an estimate of the phase difference can be made is one drive cycle and this imposes a lower limit on the effective response time of a meter. It is true that estimates could be obtained at a rate greater than is implied by this limit, if the estimates, each taken over a period of one drive cycle, use overlapping periods, but such estimates are not independent and the lower limit on the meter response time remains the period of one drive cycle. Although there may be circumstances where more closely spaced estimates are desirable, all the time histories of the phase difference in the present work are based on non-overlapping periods.

All our signal-processing algorithms were developed primarily to investigate the dynamic response of meter flow tubes. This was achieved by processing independently, either signals logged directly from flow tube sensors or simulated signals obtained from analytical and finite element studies. In order not to distort the information on the response, no filtering was used.

5. Results

For the purpose of comparing the analytical predictions with the finite element predictions, for the simple straight tube meter, the analytical predictions of the sensor signals were evaluated to give time histories equivalent to those obtained from the finite element simulations. In the evaluation it was assumed that t_0 was large so that the oscillations arising from the start-up conditions had completely decayed before the step was initiated. The analytical and finite element data streams were then subjected to identical processing to yield the time histories of the phase difference, using algorithms developed at Brunel for processing data obtained from our experiments.

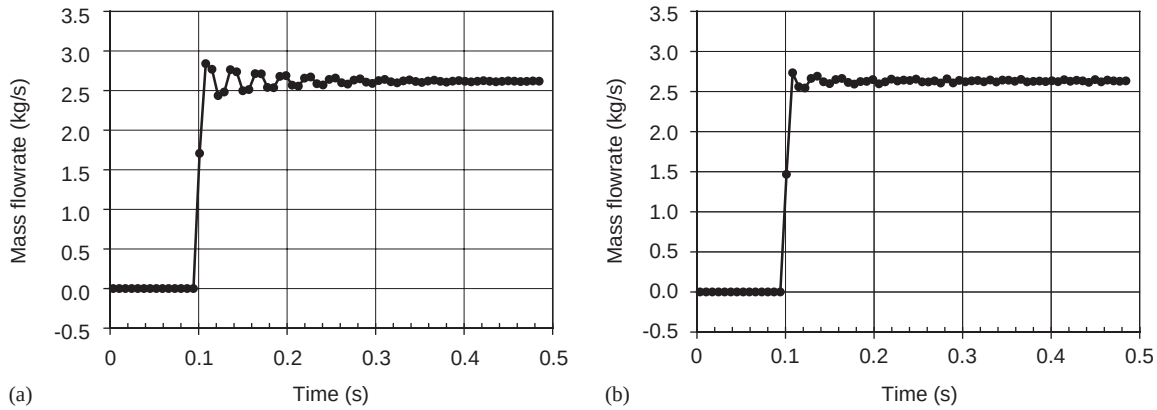

Fig. 2. Flow step from zero to 2.52 kg/s, damping 0.15%. (a) Analytical prediction. (b) Finite element prediction.

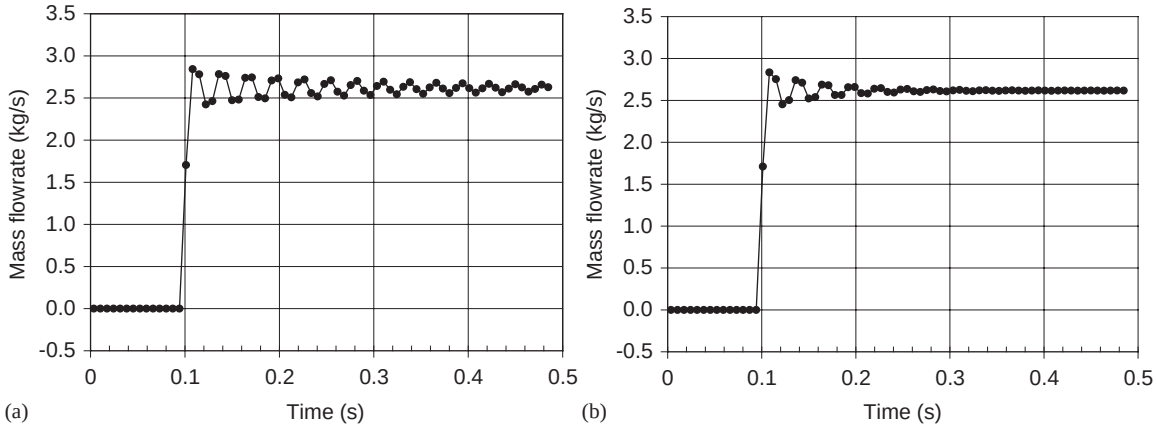

Fig. 3. The effect of changing the damping, theoretical prediction. (a) Damping 0.05%. (b) Damping 0.45%.

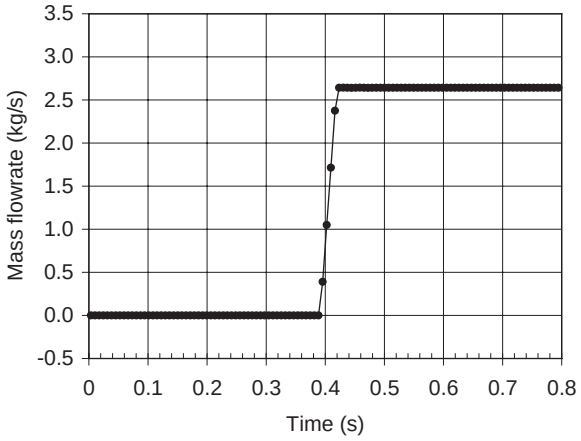

Fig. 4. Response to a 'slow' step, finite element prediction, damping 0.15%.

In order to facilitate comparisons between the analytical and finite element predictions, and experimental data, for different meters, the results are all expressed in terms of mass flow rates, assuming that there is a linear relationship between phase difference and mass flow rate. For the analytical and finite element data the empirical coefficient defining this linear relationship was determined from the mass flow rate used in the generation of the data during a period of steady flow and the mean phase difference obtained over that period. For the simple straight tube meter the coefficients derived from the analytical and the finite element results agreed within better than 1%. The experimental tests on each different meter included calibration tests at three different flow rates and the calibration coefficients were determined from the results of these tests.

Fig. 2(a) and (b) show a comparison of the response to a step as predicted by the analysis and the finite element simulation, respectively, using in both cases the experimentally determined value of the damping factor (0.15%). It should be noted that the analytical step is instantaneous, as given by the Heaviside step function where as the finite element step occurs over one calculation time step (50 μs). The two predictions of the phase difference (mass flow rate) show good agreement with respect to the decay rate, with the analytical prediction showing a larger initial amplitude of fluctuation as might be expected from the above noted difference in the detailed representation of the steps.

Figs. 3(a) and (b) show the effect on the response of increasing the damping. The data were obtained from the analytical solution but the trends would have been exactly the same if the data had been taken from finite element simulations of the straight tube meter. Fig. 3(a) uses data evaluated for a damping ratio of 0.05% (i.e. 3 times smaller than that used in Fig. 2(a)) and Fig. 3(b) uses data for a damping ratio of 0.45% (i.e. 3 times larger).

It was not considered to be practicable to attempt an analytical solution for a slower step but the finite element simulation was repeated for a step which occurred linearly over a period equal to four cycles of the meter drive. Fig. 4 shows the result of the finite element simulation (damping ratio 0.15%) and this may be compared to the simulation of a

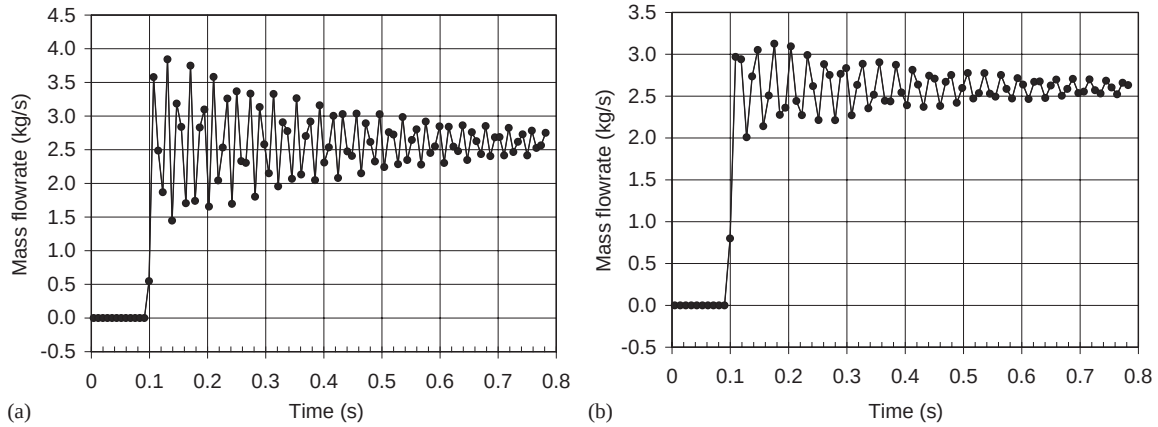

Fig. 5. Finite element predictions of response to a fast step. (a) α-Tube meter, experimentally determined damping. (b) Ω-Tube meter, experimentally determined damping.

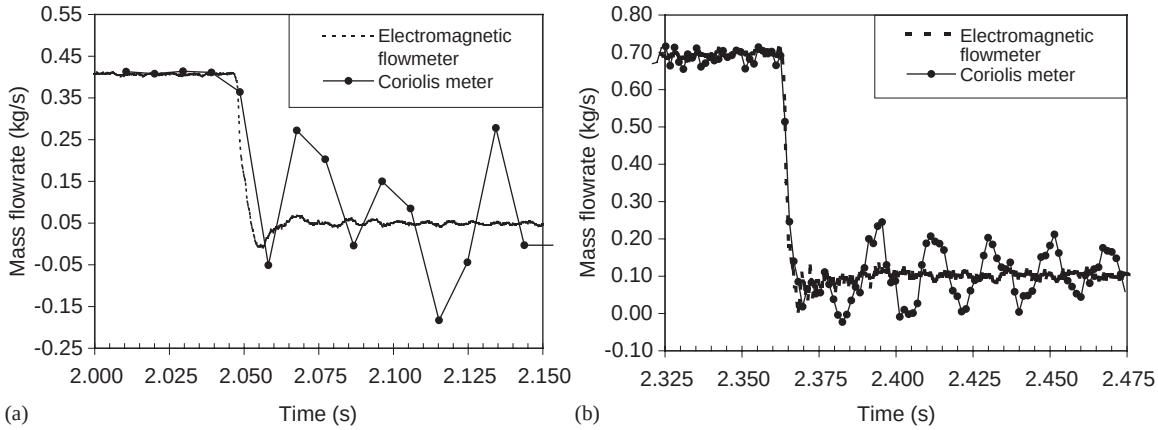

Fig. 6. Experimentally measured response to a fast step (5 ms). (a) Meter having a drive frequency of about 100 Hz. (b) Meter having a drive frequency of about 800 Hz.

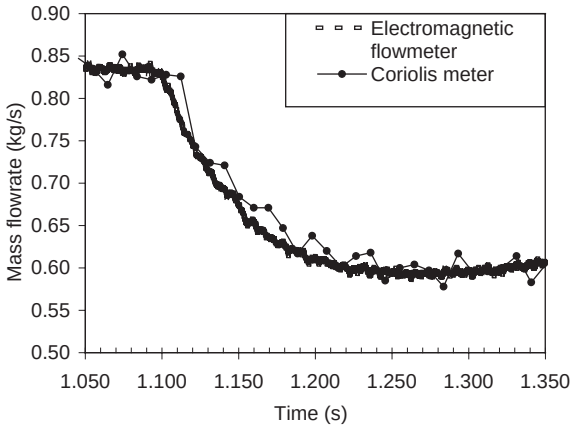

Fig. 7. Experimentally measured response to a slow step (approx. 100 ms) meter having a drive frequency of approximately 100 Hz.

fast step shown in Fig. 2(b). It is clear that no 'noise' is apparent on the time history of the phase difference (mass flow rate).

Figs. 5(a) and (b) show the finite element predictions for the responses of the α-tube and the Ω-tube meters, respectively, to a 'fast' step (one finite element calculation time step), using in each case the experimentally determined damping factor. It is clear that the nature of the response is not significantly affected by the meter geometry.

The analytical and finite element predictions can be compared with experimental measurements of the response made on a range of commercial meters. Figs. 6(a) and (b) show two examples of meter response to a fast step (5 ms duration). The data presented in Fig. 6(a) were obtained with a meter having a relatively low drive frequency (in the region of 100 Hz) while those in Fig. 6(b) were obtained with a meter having a much higher drive frequency (in the region of 800 Hz). The respective spacing of the Coriolis meter data in the two figures reflects the fact that one estimate of the phase difference (and hence of the flow rate) is obtained for each cycle of the meter drive. With the lower frequency meter the step is completed within less than one drive cycle, but with the higher frequency meter it extends over approximately three drive cycles. For both meters the noise level after the step is significantly greater than would have been predicted by a finite element simulation of a step of the same speed. That this was due to the mechanical vibrations caused by the operation of the variable area orifice device was confirmed by examination of the time history of the signal from an accelerometer attached to the apparatus.

The significance of any vibration introduced by the mechanism used for the creation of a step is further emphasized in Fig. 7 which shows the response of a meter to slow step initiated by the bursting of a diaphragm. This mechanism produces no significant mechanical vibration and the response shows no significant increase in the noise level on the Coriolis meter output signal, after the step.

6. Discussion

The data presented in Figs. 2–4 are only a part of the results derived from the analysis and the finite element modelling for the simple straight tube meter. Over the totality of the results, the agreement between the predictions of the two approaches is very good. A comparison of Figs. 3(a) and (b), together with Fig. 2(a) is interesting because it shows, as expected, that increasing the damping affects the rate of decay of the fluctuations in the computed flow rate. These fluctuations which appear to be at frequencies in the range of 40–60 Hz actually arise from the sensor signal components at the Coriolis frequency which are generated by the step. In the calculation of the phase difference at the drive frequency (between the simulated sensor signals), the Coriolis frequency component generates a beat with a frequency equal to the difference between the Coriolis frequency and the drive frequency. This frequency is much greater than the frequency at which the phase difference data are generated (i.e. the drive frequency), and so aliasing occurs, giving the impression of a lower frequency. The calculation time step used in the finite element simulation was sufficiently small for the simulated sensor signals to have shown a component at the next highest mode frequency if one had been present. Spectra of the simulated sensor signals immediately after the step, clearly show the component at the Coriolis frequency but they do not show anything at the next higher mode frequency. This provides an additional justification of the decision to truncate the analytical solution after the second mode.

For the complex geometry meters, the distribution of the modal frequencies was more complicated and for at least one of the meters, the finite element simulation showed indications that the step may generate components at frequencies other than the Coriolis frequency. However, these components were very much smaller than those at the Coriolis frequency.

In assessing the results presented in this paper for commercial meters, it is important to remember that our signal processing algorithms were developed primarily to investigate the dynamic response of meter flow tubes. This was achieved by processing independently the signals logged directly from the flow tube sensors. In order to preserve the information available within the phase difference data, no filtering was used. Further, because these data were all post-processed, the computational time required to produce the phase difference estimates was not an issue.

The signal processing requirements for the user-output of a commercial meter are significantly different from those specified above. In particular, filtering may be used to remove signal noise and the computational time required for on-line processing is a significant issue. Also, it is common for blocks of data from several (or many) drive cycles to be used in the estimation of the phase difference. In general, the differences observed between the user-output response to a fast flow step and the flow tube responses reported herein are as follows: the user-output shows a delay in the onset of the step, a lengthening of the step duration, and no fluctuations following the step.

The analytical and finite element results, together with the experimental data on the response of commercial meters to a fast step, all combine to emphasise that the time constant for the mechanical response of Coriolis meters is the period of one cycle of the drive. The very much larger time constants which are observed from the indicated output of

commercial meters (as indicated for example by Wiklund and Peluso, 2002) arise from constraints introduced by particular algorithms used for the estimation of the phase difference and from other characteristics of the signal processing. It would appear to be probable that a significant part of the increase in the time constant arises from damping introduced during the signal processing to suppress the fluctuations caused by the Coriolis frequency components in the sensor signals. It is likely that the overall design of a meter will always involve a compromise between absolute accuracy (freedom from spurious fluctuations) and speed of response. For many applications the emphasis is towards a high accuracy of mean flow indication over periods of many drive cycles. The present work has established the ultimate response time limitations.

7. Conclusions

The time constant of a Coriolis meter cannot be less than the period of one cycle of the meter drive because this is the shortest period over which a meaningful estimate of the phase difference between the sensor signals can be made.

The response of the meter sensor signals to a step change in mass flow rate comprises two parts. That part of the signal which is at the drive frequency and is responsible for the phase difference (linearly proportional to the mass flow rate) is, to a high degree of approximation, independent of the magnitude of the internal damping. There is an additional component of the response which is predominantly at the Coriolis frequency and this part decays exponentially under the influence of the internal damping.

The effective time constant of commercial Coriolis meters is generally many times larger than the period of one drive cycle because of the particular algorithms used in the determination of the phase difference and because of additional computational damping introduced to minimize the influence of the non-drive frequency components of the sensor signals.

For changes in flow rate which occur continuously over periods which are several times larger than the period of one drive cycle the Coriolis meter has the potential to measure a true time history of the change in flow rate.

Acknowledgements

The work reported in this paper was performed with the support of the Engineering and Physical Sciences Research Council of the United Kingdom. The test meters, together with the details required for the finite element modelling, were provided by their respective manufacturers and their support is gratefully acknowledged.

References

Belhadj, A., Cheesewright, R., Clark, C., 2000. The simulation of Coriolis meter response to pulsating flow using a general purpose F.E. code. Journal of Fluids and Structures 14, 613–634.

Cheesewright, R., Clark, C., 1998. The effect of flow pulsations on Coriolis mass flow meters. Journal of Fluids and Structures 12, 1025–1039.

Cheesewright, R., Clark, C., 2000. The dynamic response of Coriolis mass flow meters. Proceedings of FLUCOME'2000, Sherbrook, Canada, August, 2000.

Cheesewright, R., Clark, C., Bisset, D., 1999. Understanding the experimental response of Coriolis massflow meters to flow pulsations. Flow Measurement and Instrumentation 10, 207–215.

Cheesewright, R., Belhadj, A., Clark, C., 2003. Effect of mechanical vibrations on Coriolis mass flow meters. Journal of Dynamic Systems, Measurement, and Control 125, 103–113.

Clark, C., Cheesewright, R., 2003. The influence upon Coriolis mass flow meters of external vibrations at selected frequencies. Flow Measurement and Instrumentation 14, 33–42.

Clough, R.W., Penzien, J., 1975. Dynamics of Structures. McGraw Hill, New York.

Cunningham, T., 1994. Zero shifts in Coriolis sensors due to imbalance. AIAA Tech. Paper, AIAA-94-1621.

Hulbert, G.M., Darnell, I., Brereton, G.J., 1995. Numerical and experimental analysis of Coriolis mass flowmeters. AIAA Technical Paper, AIAA-95-1384-CP.

Paidoussis, M.P., Issid, N.T., 1974. Dynamic stability of pipes conveying fluid. Journal of Sound and Vibration 33, 267–294.

Raszillier, H., Durst, F., 1991. Coriolis-effect in mass flow metering. Archives of Applied Mechanics 61, 192–214.

Raszillier, H., Alleborn, N., Durst, F., 1993. Mode mixing in Coriolis flowmeters. Archives of Applied Mechanics 63, 219–227.

Stack, C.P., Garnett, G.E., Pawlas, G.E., 1993. A finite element for the vibration analysis of a fluid-conveying Timoshenko beam. AIAA Technical Paper, AIAA-93-1552-CP, AIAA/ASME Structures, Structural Dynamics and Materials Conference.

Wiklund, D., Peluso, M., 2002. Quantifying and specifying the dynamic response of flowmeters. ISA2002 Technical Conference, Chicago, USA.